Article

Journal of
Nanoscience and Nanotechnology
Vol. 14, 9178–9181, 2014
www.aspbs.com/jnn

Hierarchical Porous Carbon/MnO_2 Hybrids as Supercapacitor Electrodes

Min Eui Lee, Young Soo Yun, and Hyoung-Joon Jin*

Department of Polymer Science and Engineering, Inha University, Incheon 402-751, Republic of Korea

Hybrid electrodes of hierarchical porous carbon (HPC) and manganese oxide (MnO_2) were synthesized using a fast surface redox reaction of potassium permanganate under facile immersion methods. The HPC/MnO_2 hybrids had a number of micropores and macropores and the MnO_2 nanoparticles acted as a pseudocapacitive material. The synergistic effects of electric double-layer capacitor (EDLC)-induced capacitance and pseudocapacitance brought about a better electrochemical performance of the HPC/MnO_2 hybrid electrodes compared to that obtained with a single component. The hybrids showed a specific capacitance of 228 F g^{-1} and good cycle stability over 1000 cycles.

Keywords: Porous Carbons, Manganese Oxide, Hybrids, Supercapacitor.

1. INTRODUCTION

Supercapacitors have attracted increasing attention because they have higher power density and longer cycle ability than rechargeable batteries.[1] Supercapacitors can be classified according to their energy-storage mechanism into two categories: electric double-layer capacitors (EDLCs) and pseudocapacitors. EDLCs come from the pure electrostatic charge accumulated at the electrode/electrolyte interface. Therefore, EDLCs exhibit good cycle stability and high power density. However, EDLCs require an electrode with a high specific surface area and pores of size of the ions.[2] Other category is pseudocapacitors, in which fast and reversible faradic processes take place due to an electro-active species. Transition-metal oxides such as ruthenium oxide (RuO_2) or manganese oxide (MnO_2) and electrically conductive polymers have been used as pseudocapacitive electrode materials.[3] In particular, MnO_2 has drawn much attention as a pseudocapacitive electrode material for supercapacitors owing to its low cost, natural abundance, environmental compatibility, and high theoretical specific capacitance ($\sim$1100 F g^{-1}).[4] However, the poor cycle stability and low electrical conductivity of MnO_2 have limited its practical application as a pseudocapacitive material.[5]

Recently, carbon-based materials with pseudocapacitive effects have been reported.[6–8] Carbon-based materials containing electro-active heteroatoms have exhibited great improvement of the specific capacitance owing to both EDLC-induced capacitance and the pseudocapacitive effect. These results suggest that hybrids based on carbon-based materials with a high specific surface area and a metal oxide can be a superior electrode material. In this study, we made macroporous carbon-based material from cellulose.[9] The carbon pores are totally open and interconnected, which is advantageous in terms of mass transfer of the reactants.[10, 11] These porous structures can provide highly efficient electroytle-ion transport through the macropores, micropores and mesopores. The hierarchical porous carbon (HPC), which has a high surface area and a macroporous structure, was selected as a part of the electrode, with pseudocapacitive MnO_2 nanoparticles homogeneously incorporated on the surface of HPC. The HPC/MnO_2 nanoparticle hybrid electrodes exhibited a better electrochemical performance by synergistic effects induced by its EDLC-based and its pseudocapacitive performance.

2. EXPERIMENTAL DETAILS

2.1. Preparation of HPC/MnO_2 Hybrids

HPC was prepared using a previously reported procedure, in which a mixture of 7 wt% NaOH, 12 wt% urea, and 81 wt% water was prepared and pre-cooled to − 12 °C for 2 h. Then, 4 wt% cotton cellulose (Aldrich) was immersed in the mixture solution, which was then vigorously stirred

*Author to whom correspondence should be addressed.

1533-4880/2014/14/9178/004 doi:10.1166/jnn.2014.10086

for approximately 5 min at room temperature. The mixture solution was frozen at −196 °C and then freeze-dried for 3 days. The resulting cryogel was carbonized by heating from room temperature to 700 °C for 2 h at a heating rate of 10 °C/min and an Ar flow rate of 200 mL/min. The solution was then washed using distilled water and ethanol and dried in a vacuum oven at 30 °C for 24 h. The carbon material was ground and added into 200 mL of a 2 mM $KMnO_4$ solution under continuous stirring at 70 °C for 5 min. After the reaction was completed, the sample was washed using distilled water and ethanol to eliminate unreacted MnO_4^- and dried in an oven at 60 °C.

2.2. Characterization

The morphology of the hybrid samples was observed using transmission electron microscopy (TEM, CM200, Philips). X-ray diffraction (XRD, Rigaku DMAX-2500) analysis of the samples was performed using Cu Kα radiation (wavelength $\lambda = 0.154$ nm) operated at 40 kV and 100 mA. X-ray photoelectron spectroscopy (XPS, AXIS-HIS, Kratos Analytical, Japan) was performed using monochromated Mg Kα radiation ($h\upsilon = 1500$ eV). A two-electrode cell configuration was used to measure the performance of the samples as electrodes for supercapacitors. For the aqueous system, 5 wt% polytetrafluoroethylene (PTFE, Sigma-Aldrich, 60 wt% dispersion in H_2O) was added to the samples as binder. Typically, the samples and PTFE were mixed to form a paste using a mortar and pestle, rolled into sheets of uniform thickness whit a thickness range from 40 to 50 μm (from sheet to sheet), and punched into 1×1 cm diameter electrodes. A typical pair of electrodes had a weight between 2.5 and 3.0 mg after drying overnight at 100 °C. 0.5 M Na_2SO_4 (Sigma-Aldrich, 99%) was used as aqueous electrolyte. The electrodes and a porous polypropylene separator (Whatman GF/B) were sandwiched together in a

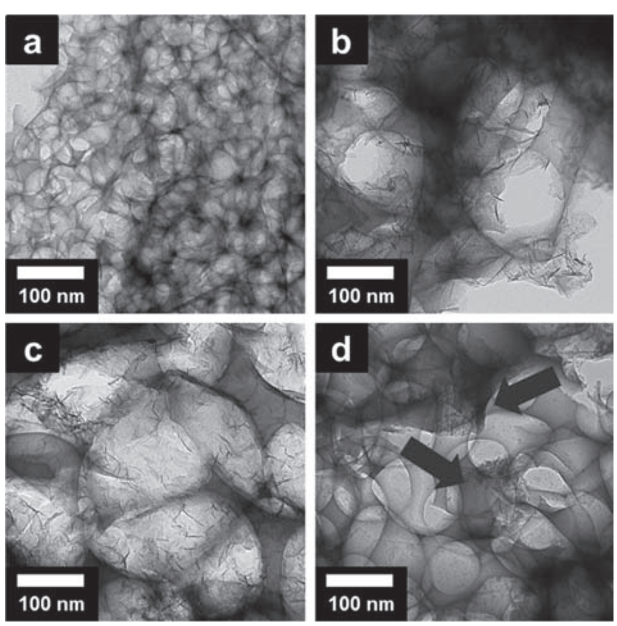

Figure 1. TEM images of (a) HPC and HPC/MnO_2 hybrids with reaction times of (b) 30 s, (c) 5 min, and (d) 10 min (the arrows are a state in which the manganese oxide is aggregated).

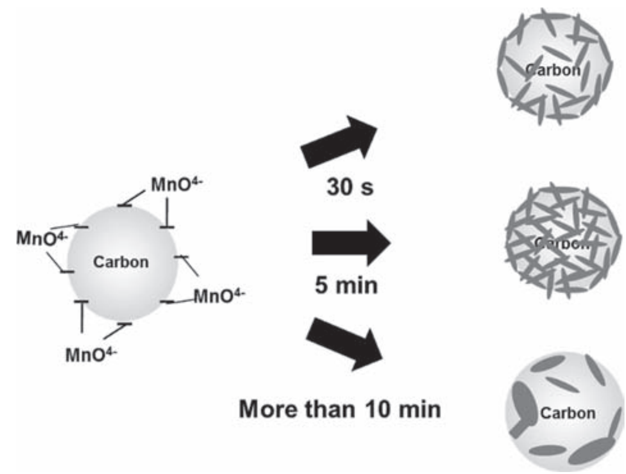

Figure 2. Schematic diagram of HPC/MnO_2 hybrids fabricated using different reaction times.

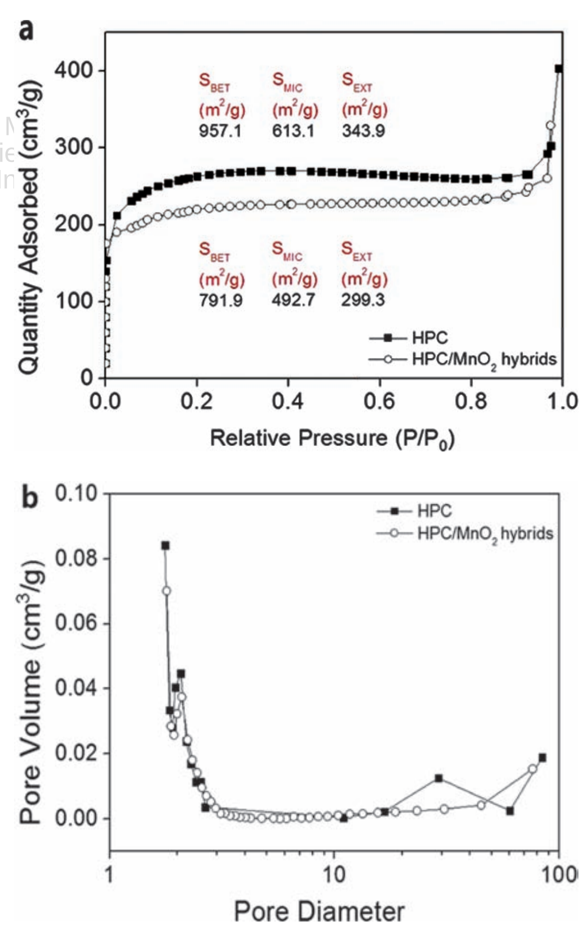

Figure 3. (a) Nitrogen adsorption and desorption isotherm curves and (b) pore size distribution of the samples (black squares: HPC, open circles: HPC/MnO_2 hybrids).

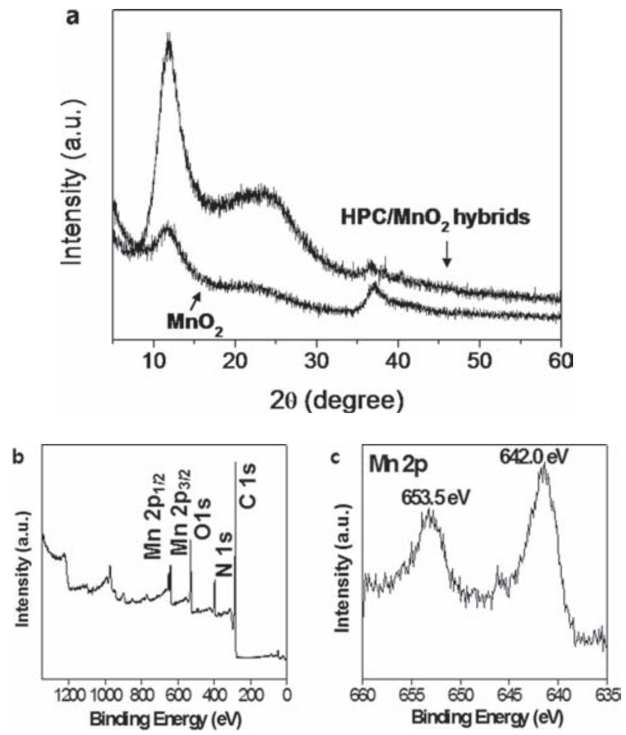

Figure 4. (a) XRD patterns of MnO_2 and HPC/MnO_2 hybrids. (b) XPS survey spectra and (c) the magnified view of the Mn 2p region of the hybrids.

stainless steel cell to accomplish the fully assembled two-electrode system. The electrochemical performances of the samples were evaluated by cyclic voltammetry (CV) and chronopotentiometry.

3. RESULTS AND DISCUSSION

The TEM image of Figure 1(a) exhibits the three-dimensional (3-D) macroporous structure of HPC. The morphology of the HPC/MnO_2 hybrids at different magnifications is shown in Figures 1(b) and (c). It can be seen that needle-like MnO_2 is distributed on the carbon surface and inner pores. Despite the fact that $KMnO_4$ is a strong oxidizing agent, the carbon morphology was well preserved. Experimenting with different reaction times and quantities of MnO_2 [Figs. 1(b)–(d)], optimal HPC/MnO_2 hybrids were prepared. With a reaction time of 5 min and 2 mM of $KMnO_4$ at 70 °C, MnO_2 was homogeneously introduced onto the surface of HPC [Fig. 1(c)]. Figure 2 shows a schematic image of the HPC/MnO_2 hybrids fabricated with different reaction times. The pore characteristics of HPC and HPC/MnO_2 are shown in Figures 3(a), (b). Nitrogen adsorption and desorption isotherms of HPC and HPC/MnO_2 showed IUPAC type-I and IV hybrid shapes. The surface area of HPC is 957.1 m^2 g^{-1}, which means that the surface areas of micropores (613.1 m^2 g^{-1}) are twice as large as that of mesopores (343.9 m^2 g^{-1}). In the case of HPC/MnO_2, the surface area was 651 m^2 g^{-1}, which means that the surface areas of micropores (410.9 m^2 g^{-1}) and mesopores (240.1 m^2 g^{-1}) make up. Although the surface area of HPC/MnO_2 was reduced by MnO_2 on carbon, synergistic effects of HPC and MnO_2 were observed by maintaining the pore structure, which incresed the capacitance of the HPC/MnO_2 hybrids in comparison to sole HPC.[12] Figure 4(a) shows typical XRD patterns of the as-prepared MnO_2 and HPC/MnO_2 hybrids. The presence of HPC and

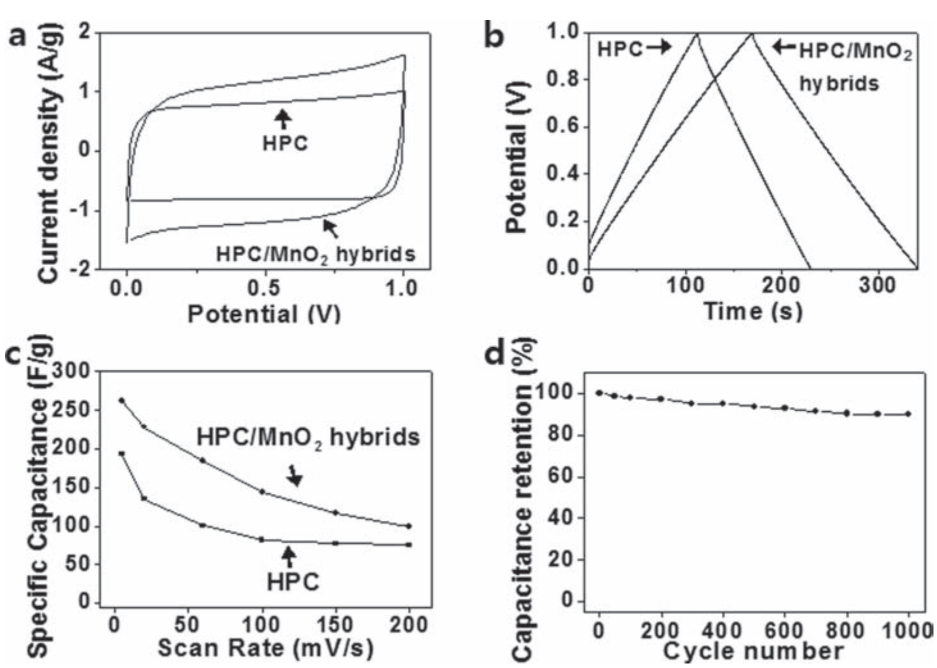

Figure 5. Cyclic voltammograms of HPC and HPC/MnO_2 hybrids at a scan rate of 10 mV s^{-1}. (b) Galvanostatic charge/discharge curve of the HPC/MnO_2 hybrids at a current density of 1 A g^{-1} in a potential window of 0 to 1.0 V. (c) Specific capacitances of HPC and HPC/MnO_2 hybrid electrodes as a function of scan rates. (d) Cyclic stability of the HPC/MnO_2 hybrid electrodes at a scan rate of 50 mV s^{-1} over 1000 cycles.

MnO_2 in a mixed crystalline or amorphous structure was confirmed from the XRD patterns.[14] The two broad peaks at around 12° and 37° can be indexed according to MnO_2. The carbon peak appeared at around 26°, with a second broad, weak peak at around 44°, which is characteristic of graphitic carbon. In this sample, the three peaks around 12°, 26°, and 37° were assigned to the crystal planes (110), (002), and (211) of α-MnO_2, respectively.[13] The XRD pattern of the HPC/MnO_2 hybrids shows an amorphous structure. The chemical configurations of the HPC/MnO_2 hybrids were characterized by XPS. The peaks of Mn ($2p_{3/2}$, $2p_{1/2}$), O 1s, and C 1s are shown in the survey spectrum [Fig. 4(b)]. The Mn $2p_{3/2}$ peak is centered at 642.1 eV and the Mn $2p_{1/2}$ peak at 653.8 eV, which is in good agreement with the reported data for Mn $2p_{3/2}$ and $2p_{1/2}$ in MnO_2 [Fig. 4(c)].[15] The XPS data coincide with the XRD data.

The evaluation of the electrochemical performance of the HPC/MnO_2 hybrids was conducted in a 0.5 M Na_2SO_4 aqueous electrolyte. Figure 5(a) shows the CV curves of the HPC and HPC/MnO_2 hybrids over a potential range from 0 to 1 V at a scan rate of 10 mV s^{-1}. It is noticed that the curves are somewhat rectangular, which indicates almost ideal capacitance behavior. The specific capacitances of the HPC and HPC/MnO_2 hybrids were 161 and 228 F g^{-1}, respectively. The hybrid electrodes showed a capacitance that was approximately 41.6% higher than that of HPC. The galvanostatic charge/discharge curves of the HPC and HPC/MnO_2 hybrids are shown in Figure 5(b). It shows that the charging curves are symmetric with their discharging counterparts. The specific capacitances of the HPC and HPC/MnO_2 hybrids were also caculated from the galvanostatic charge–discharge curves at a discharging rate of 1 A g^{-1} and reached 110 and 180 F g^{-1}, respectively. The variation in the specific capacitance of the HMC/MnO_2 hybrids as a function of the scan rates is plotted in Figure 5(c). The specific capacitance decreased on increasing scan rates. However, the specific capacitance of the HPC/MnO_2 hybrids (103 F g^{-1}) was maintained at a relatively high scan rate of 200 mV s^{-1}. Also, across the entire range of scan rates, the HPC/MnO_2 hybrids showed higher capacitnaces than HPC. This is a result of the synergistic effects of EDLC-based HPC and the pseudocapacitive effects of MnO_2. Moreover, the HPC/MnO_2 hybrids can increase the effective contact area between MnO_2 and the electrolyte, which results in high electrochemical utilization of MnO_2. For the HPC/MnO_2 hybrids, cycling tests were carried out for 1000 cycles [Fig. 5(d)]. After 1000 cycles at a scan rate 50 mV s^{-1}, the capacitances of the HPC/MnO_2 hybrids decreased to 11% of the initial capacitance, which was attributed to HPC on covering the MnO_2 by reducing the stress and proper pore structure.

4. CONCLUSIONS

HPC/MnO_2 hybrids were prepared by using cellulose-based materials and a fast surface redox reaction of potassium permanganate under facile immersion methods. HPC/MnO_2 hybrids were prepared with 2 mM $KMnO_4$ and a reaction time of 5 min at 70 °C. The HPC/MnO_2 hybrids showed a specific capacitance of 228 F g^{-1} at a scan rate of 10 mV s^{-1}, and a specific capacitance of 103 F g^{-1} was maintained at a relatively high scan rate of 200 mV s^{-1}. Furthermore, a stable electrochemical performance was maintained for 1000 cycles.

Acknowledgments: This work was supported by the National Research Foundation of Korea Grant funded by the Korean Government (MEST) (NRF-2010-C1AAA001-0029018) and Basic Science Research Program through the National Research Foundation of Korea (NRF) funded by the Ministry of Education (2013008534), and also supported by a grant from the Technology Development Program for Strategic Core Materials funded by the Ministry of Trade, Industry and Energy, Republic of Korea (Project No. 10047758).

References and Notes

1. P. Simon and Y. Gogotsi, *Nat. Mater.* 7, 845 (**2008**).
2. Y. S. Yun, S. Y. Cho, J. Shim, B. H. Kim, S.-J. Chang, S. J. Baek, Y. S. Huh, Y. Tak, Y. W. Park, S. Park, and H.-J. Jin, *Adv. Mater.* 25, 1993 (**2013**).
3. V. Khomenko, E. Raymundo-Pinero, and F. Beguin, *J. Power Sources* 153, 183 (**2006**).
4. G. An, P. Yu, M. Xiao, Z. Liu, Z. Miao, K. Ding, and L. Mao, *Nanotechnology* 19, 275709 (**2008**).
5. Z. Li, Y. Mi, X. Liu, S. Liu, S. Yang, and J. Wang, *J. Mater. Chem.* 21, 14706 (**2011**).
6. D. Hulicova-Jurcakova, M. Seredych, G. Q. Lu, and T. J. Bandosz, *Adv. Funct. Mater.* 19, 438 (**2009**).
7. Y. S. Yun, H. H. Park, and H.-J. Joon, *Materials* 5, 1258 (**2012**).
8. M. Evans, E. Halliop, and J. Macdonald, *Carbon* 37, 269 (**1999**).
9. Y. S. Yun, J. Y. Shim, Y. S. Tak, and H.-J. Jin, *Rse Adv.* 2, 4353 (**2012**).
10. M. Lillo-Rodenas, D. Lozano-Castello, D. Cazorla-Amoros, and A. Linares-Solano, *Carbon* 39, 751 (**2001**).
11. S. B. Ma, K. Y. Ahn, E. S. Lee, K. H. Oh, and K. B. Kim, *Carbon* 45, 375 (**2007**).
12. Y. S. Yun, C. B. Im, H. H. Park, I. G. Hwang, Y. S. Tak, and H.-J. Jin, *J. Power Sources* 234, 285 (**2013**).
13. Y. U. Jeong and A. Manthriram, *J. Electrochem. Soc.* 149, A1419 (**2002**).
14. J. Yan, Z. Fan, T. Wei, J. Cheng, B. Shao, K. Wang, L. Song, and M. Zhang, *J. Power Sources* 194, 1202 (**2009**).
15. S. W. Lee, J. H. Kim, S. Chen, P. T. Hammond, and Y. Shao-Horn, *ACS Nano* 4, 3889 (**2010**).

Received: 8 April 2013. Accepted: 6 January 2014.